# Configuration-dependent band structures in odd-odd $^{180}$Ir

Y. H. Zhang,[1] T. Hayakawa,[2] M. Oshima,[2] J. Katakura,[2] Y. Hatsukawa,[2] M. Matsuda,[2] H. Kusakari,[3] M. Sugawara,[4] T. Komatsubara,[5] and K. Furuno[5]

[1]*Institute of Modern Physics, Chinese Academy of Sciences, Lanzhou 730000, China*

[2]*Japan Atomic Energy Research Institute, Tokai, Ibaraki 319-1195, Japan*

[3]*Chiba University, Inage-ku, Chiba 263-8512, Japan*

[4]*Chiba Institute of Technology, Narashino, Chiba 275-0023, Japan*

[5]*Institute of Physics and Tandem Accelerator Center, University of Tsukuba, Ibaraki 305-0006, Japan*

(Received 11 April 2001; published 3 December 2001)

High-spin states in $^{180}$Ir have been investigated by means of in-beam $\gamma$-ray spectroscopy techniques with the $^{154}$Sm($^{31}$P,5$n\gamma$)$^{180}$Ir reaction. Excitation functions, $x$-$\gamma$ and $\gamma$-$\gamma$-$t$ coincidences, DCO (directional correlation of $\gamma$ rays deexciting oriented states) ratios, and intraband $B(M1)/B(E2)$ ratios were measured. Five rotational bands have been identified and their configurations are proposed on the basis of $B(M1)/B(E2)$ ratios and by comparing the band properties with known bands in neighboring odd-mass and even-mass nuclei. The neutron $AB$ crossing is observed at $\hbar\omega_c = 0.26(1)$ MeV for the $\pi 1/2^-[541] \otimes \nu 1/2^-[521]$ and $\pi 1/2^-[541] \otimes \nu 5/2^-[512]$ bands, respectively. Staggering of levels as a function of the number of neutron pairs is revealed in the $\pi 1/2^-[541] \otimes \nu 1/2^-[521]$ doubly decoupled bands of $^{178-186}$Ir. The gradual alignment gains at low rotational frequencies are observed in the two strongly coupled bands. Band crossings and alignments in $^{180}$Ir are discussed with reference to the total Routhian surface and cranked shell model calculations performed for the neighboring odd-mass nuclei.

DOI: 10.1103/PhysRevC.65.014302 PACS number(s): 21.10.Re, 23.20.−g, 23.20.Lv, 27.70.+q

## I. INTRODUCTION

The band structures of deformed odd-odd nuclei are among the most complex encountered experimentally because of the existence of a large number of low-lying two-quasiparticle states. Studies of radioactive decay generally provide only information about low-spin levels because the even-even parents have $I=0$ ground states, whereas the heavy-ion-induced fusion-evaporation reactions populate high-spin states near the yrast line. The deexcitation of bandheads to the ground state is not known in most cases, making the spin and parity, $I^\pi$, and configuration assignments difficult. During the past two decades, great efforts have been devoted to the study of odd-odd nuclei, leading to a general classification of band structures according to the coupling scheme between the valence proton and neutron [1]. With the aid of refined in-beam spectroscopy techniques, high-quality data now make it possible to establish connections among the bands in different quasiparticle configurations. Thus the spin and parity of one band can be unambiguously fixed relative to the others. As a consequence, low-spin signature inversion [2] has been observed in the $\pi 1/2^-[541] \otimes \nu i_{13/2}$ semidecoupled bands in $^{162,164}$Tm and $^{174}$Ta [3]. This phenomenon has also been observed in $^{176}$Re [4], $^{178}$Ir [5], $^{170,172}$Ta [6,7], and $^{166,168}$Lu [8,9] and attributed to the proton-neutron residual interactions [3,4,10]. As a consequence, the spin assignments to a number of semidecoupled bands in this mass region have been reevaluated [4,11].

In contrast, the nuclei in the lighter Os-Ir-Pt regime are rather soft with respect to $\beta$ and $\gamma$ deformations, and the polarizing effects of individual nucleons make the nuclear shapes strongly configuration dependent. For a long time, one has been puzzled by the complex alignments at a frequency range of 0.20–0.35 MeV in the ground-state bands of even-even nuclei (see, for example, Ref. [12] and references therein) and in the $\pi h_{11/2}$ and $\pi d_{5/2}$ bands of odd-$A$ Re and Ir isotopes (see, for example, Ref. [13] and references therein). Different mechanisms may be associated with this phenomenon, such as strong interactions at a band crossing [12], shape change with rotation [14], $(\pi h_{9/2})^2$ alignment [15], and reduced $(\nu i_{13/2})^2$ alignment [16] as well as the combined results of $(\pi h_{9/2})^2$ and $(\nu i_{13/2})^2$ alignments [15]. The three-band model has also been used frequently [13] to explain the complex alignment patterns. The high-spin band structures in the odd-odd nuclei may shed light on this problem since here one can block one or two sensitive orbitals, thus reflecting the effects of an individual orbital in the band structures.

In this article, we report experimental results on high-spin band structures in odd-odd $^{180}$Ir. The experimental details and data analyses will be described in Sec. II. The configuration assignments to rotational bands, as presented in Sec. III, are suggested according to the measured in-band $B(M1)/B(E2)$ ratios and the existing knowledge of band properties in neighboring odd-mass and even-mass nuclei. The configuration-dependent alignment patterns are qualitatively discussed for lighter Os and Ir isotopes in terms of total Routhians surface (TRS) and cranked shell model (CSM) calculations. Prior to this work, no high-spin data on $^{180}$Ir have been available in the literature. The ground state of $^{180}$Ir was suggested to be $I^\pi = (4,5)^+$ from the study of $^{180}$Ir $\beta^+$/EC decay [17]. From $^{184}$Au $\alpha$-decay studies four low-lying excited states in $^{180}$Ir have been identified, but without the spin and parity assignments [18]. A preliminary report of this work has been published elsewhere [19].

 

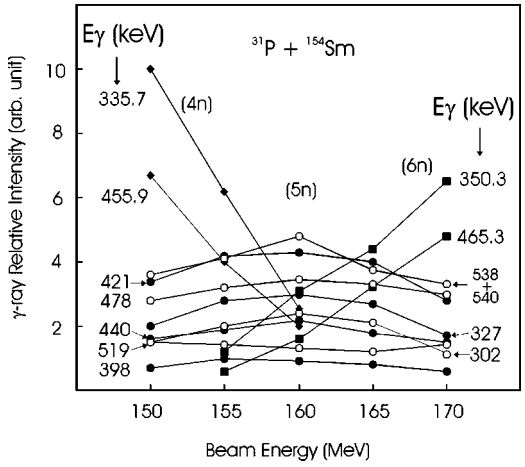


FIG. 1. Excitation functions for some uncontaminated $\gamma$ rays.

## II. EXPERIMENTS AND RESULTS

### A. Measurements

The experiment was performed at the Japan Atomic Energy Research Institute (JAERI). The $^{154}$Sm($^{31}$P,5$n\gamma$)$^{180}$Ir reaction was induced by a $^{31}$P beam provided by the JAERI tandem accelerator. The target was an enriched $^{154}$Sm metallic foil of 2 mg/cm$^2$ thickness backed with a 5 mg/cm$^2$ evaporated Au layer. A $\gamma$-ray detector array [20] comprising 12 HPGe's with BGO anti-Compton (AC) shields was used; six detectors had an efficiency of 40% each and the others had 70% relative to 3″×3″ NaI. The detectors were calibrated with $^{60}$Co, $^{133}$Ba, and $^{152}$Eu standard sources; typical energy resolution was about 2.0–2.4 keV at full width at half maximum (FWHM) for the 1332.5 keV line.

In order to identify the in-beam $\gamma$ rays belonging to $^{180}$Ir, we measured an excitation function by varying the $^{31}$P beam from 150 MeV to 170 MeV with 5-MeV energy steps. The $\gamma$ spectrum in this experiment was very complex; the photon peaks were often doublets or contaminated by the decay $\gamma$ rays from other reaction channels. Therefore we used a coincidence mode in the excitation function measurements so that the low-multiplicity $\gamma$ rays could be suppressed. In Fig. 1, we present some of the $\gamma$-ray intensities, normalized to the same beam current, as a function of beam energy. As shown in the figure, the $\gamma$ rays emanating from $^{179}$Ir (350- and 465-keV lines) [21] and $^{181}$Ir (336- and 456-keV lines) [22] can be clearly separated from those of $^{180}$Ir (5$n$ reaction channel).

A beam energy of 160 MeV was used during $x$-$\gamma$-$t$ and $\gamma$-$\gamma$-$t$ coincidence measurements. The time window for $\gamma$-$\gamma$ coincidence was set to be 200 ns. About 240×10$^6$ coincidence events were accumulated and sorted into a 4$k$×4$k$ matrix for off-line analysis. The relatively intense $\gamma$ rays were from the fusion-evaporation residues of $^{179,180,181}$Ir, $^{180}$Os, and $^{177}$Re corresponding to 6$n$,5$n$,4$n$,4$np$, and $\alpha$3$n$ evaporation channels, respectively. Fortunately, detailed high-spin level schemes for $^{179,181}$Ir, $^{180}$Os, and $^{177}$Re are available [21–24]. This information and the coincidences we

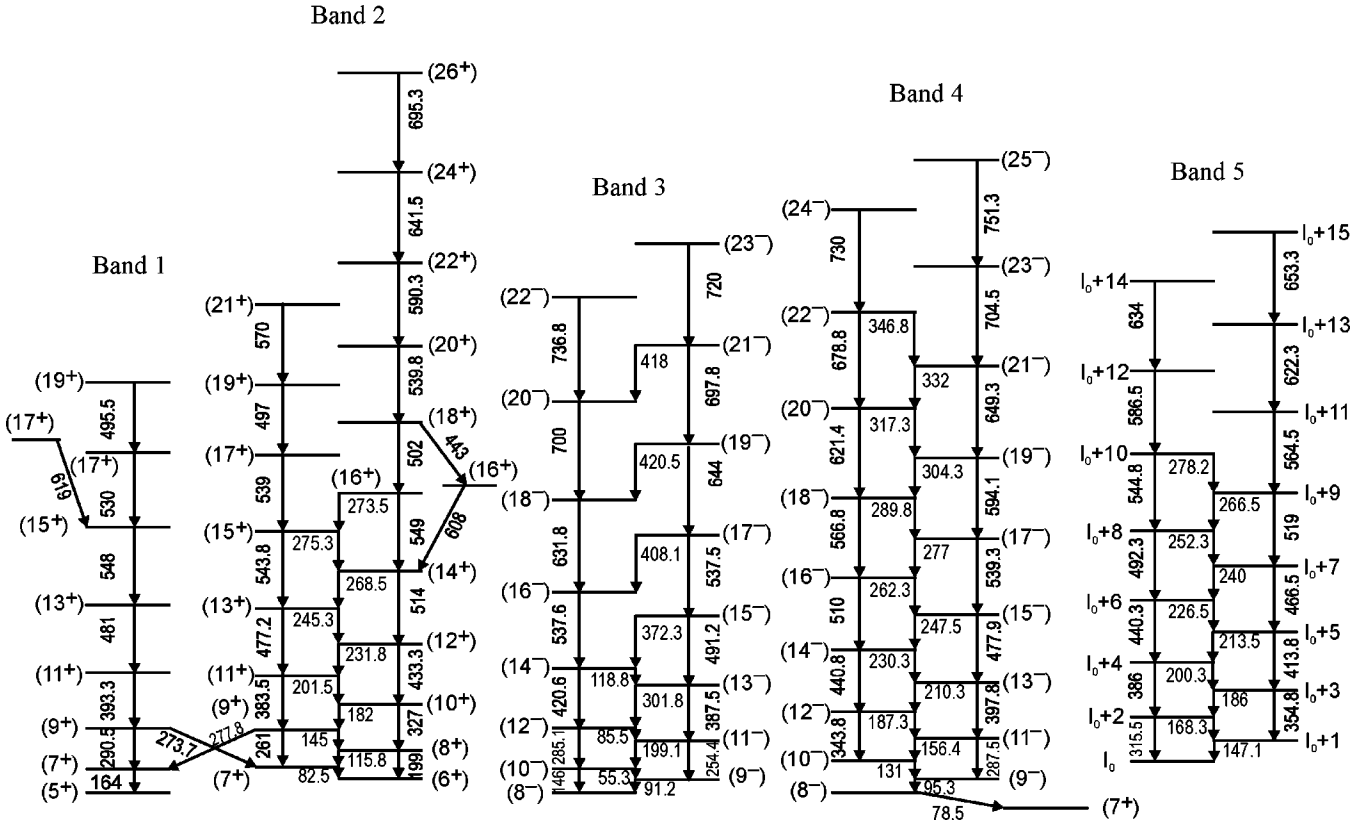


FIG. 2. Level scheme of $^{180}$Ir deduced from the present work. The relative energies of the bands are arbitrary since the connections of bandheads with the ground state have not been established.

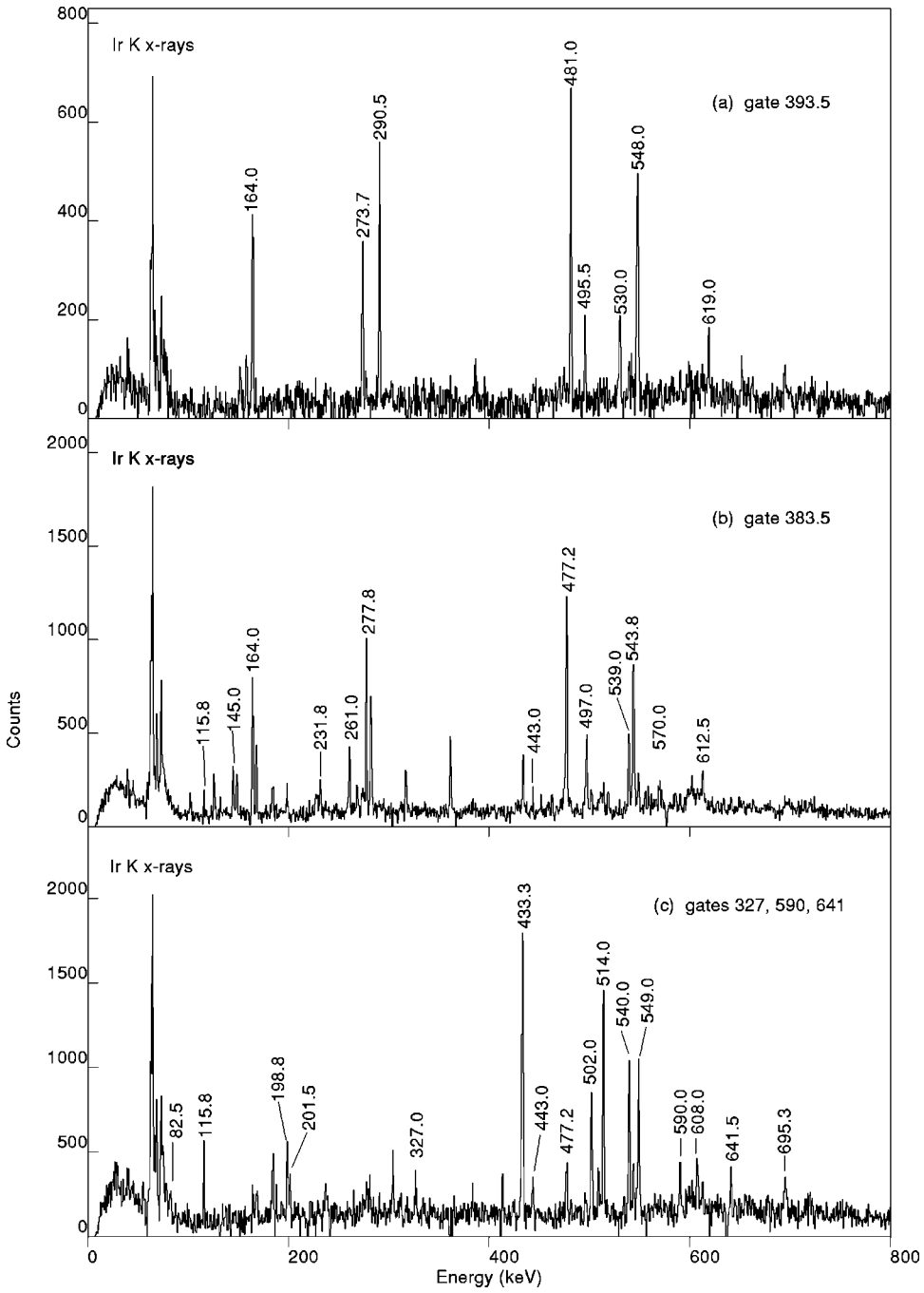


FIG. 3. Typical coincidence spectra with gates on selected transitions in bands 1 and 2 as indicated on the panels.

measured with Ir K x rays helped us assign new rotational bands in $^{180}$Ir.

To obtain the DCO (directional correlation of $\gamma$ rays deexciting oriented states) ratios, the detectors were divided into three groups positioned at 32° (148°), 58° (122°), and 90° with respect to the beam direction. A nonsymmetrized matrix with detectors at $\theta_2 = 90°$ against those at $\theta_1 = 32°$ (and $\pm 148°$) was constructed. The experimental DCO ratio was calculated by $R_{DCO}(\gamma) = I_\gamma(\theta_1)/I_\gamma(\theta_2)$, where $I_\gamma(\theta_1)$ represents the intensities of an unknown $\gamma$ ray along the $\theta_1$ axis in coincidence with the stretched $E2$ transitions along $\theta_2$ direction. Similarly, with the same gates on the $\theta_1$ axis, coincidence spectra along the $\theta_2$ axis were projected to determine $I_\gamma(\theta_2)$. Usually a single gate above the state of interest was used. For some weak transitions several $E2$ transitions in cascade were used as gates to get high statistics. In the present geometry, stretched quadrupole transitions were adopted if $R_{DCO}(\gamma)$ ratios were close to unity, and dipole transitions were assumed if $R_{DCO}(\gamma) \leqslant 0.6$.

### B. Level scheme

The level scheme of $^{180}$Ir deduced from the present work is shown in Fig. 2. The relative positions of the bands are not known (with the exception of band 1 and band 2) as neither interband transitions nor transitions from these bands to the ground state could be fully established. The ordering of transitions in each band is proposed according to the $\gamma$-ray rela-

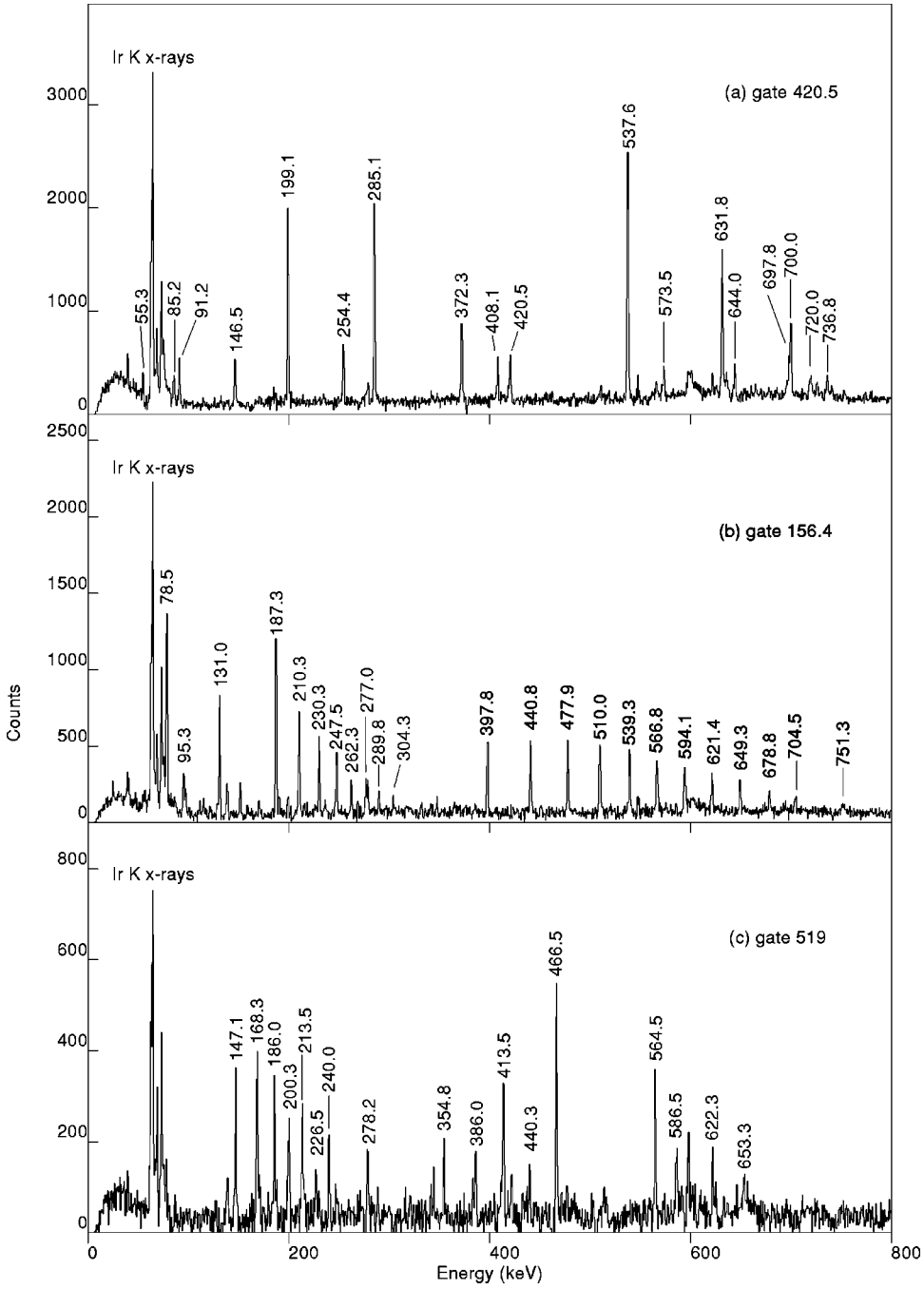


FIG. 4. Typical coincidence spectra with gates on selected transitions in bands 3, 4, and 5 as indicated on the panels.

tive intensities, $\gamma$-$\gamma$ coincidence relationships and $\gamma$-ray energy sums. Typical gated spectra are shown in Figs. 3 and 4 where the $\gamma$ transitions belonging to each band are indicated by the $\gamma$-ray energies (in keV).

The linking transitions of 273.7-keV [from $(9^+)$ of band 1 to $(7^+)$ of band 2] and 277.8-keV [from $(9^+)$ of band 2 to $(7^+)$ of band 1] lines are emphasized in Figs. 3(a) and 3(b). The main contaminant lines in Fig. 3(b) are from $^{179}$Ir [21]; in particular, the 497-keV line is heavily contaminated by the $33/2^+ \rightarrow 29/2^+$ transition in the $\pi 1/2^+[660]$ band of $^{179}$Ir. However, from the intensity-balance argument, the main part of the 497-keV line in Fig. 3(b) should be due to the $(19^+) \rightarrow (17^+)$ transition in band 2. The highest-spin transition (695.3-keV line) in band 2 can be clearly seen in the summed coincidence spectrum of Fig. 3(c). Low-energy transitions in band 3 (55.3-, 85.5-, and 91.2-keV lines) can be seen clearly in Fig. 4(a). Both the 78.5- and 95.3-keV $\gamma$ rays coincide strongly with the in-band transitions in band 4. Assuming pure $M1$ character for the 131-keV $\gamma$ transition, we calculate the total conversion coefficient to be $\alpha_T(131\ \text{keV};\ M1) = 2.93$. From the 156-keV gated spectrum [Fig. 4(b)], the $\gamma$-ray intensity ratio $R = I_\gamma\ (131\ \text{keV})/I_\gamma(95.3\ \text{keV})$ has been extracted to be 2.28(0.57), indicating an experimental conversion coefficient, $\alpha_T(95.3\ \text{keV}) = [1 + \alpha_T(131\ \text{keV};\ M1)] \times R - 1 = 8.0(2.0)$. This total conversion coefficient is very close to the theoretical value of 7.4 for a 95.3-keV $M1$ transition. Therefore, the 95.3-keV line is assigned to feed the bandhead $(8^-)$ of band 4. In the same way, the $\gamma$-ray

intensity ratio $R=I_\gamma$ (95.3 keV)/$I_\gamma$ (78.5 keV) has been extracted to be 0.23(0.05), leading to $\alpha_T$ (78.5 keV) $=0.89(0.20)$. This value agrees with the theoretical calculation of 0.75 for a 78.5-keV $E1$ transition; therefore the 78.5-keV $\gamma$ ray is proposed to feed to the $(7^+)$ state as shown in Fig. 2.

For the four rotational bands shown in Fig. 2, the branching ratios, which are defined as

$$\lambda=\frac{T_\gamma(I\to I-2)}{T_\gamma(I\to I-1)}, \tag{1}$$

were extracted for most transitions. Here $T_\gamma(I\to I-2)$ and $T_\gamma(I\to I-1)$ are the $\gamma$-ray intensities of the $\Delta I=2$ and $\Delta I=1$ transitions, respectively. These intensities are measured in a summed coincidence spectrum gated by the transitions above the state of interest. The branching ratios were used to extract the reduced transition probability ratios, which are defined as

$$\frac{B(M1,I\to I-1)}{B(E2,I\to I-2)}=0.697\frac{[E_\gamma(I\to I-2)]^5}{[E_\gamma(I\to I-1)]^3}\frac{1}{\lambda}\frac{1}{1+\delta^2}\left(\frac{\mu_N^2}{e^2b^2}\right), \tag{2}$$

where $\delta$ is the $E2/M1$ mixing ratio for the $\Delta I=1$ transitions, and $E_\gamma(I\to I-1)$ and $E_\gamma(I\to I-2)$ are the $\Delta I=1$ and $\Delta I=2$ transition energies, respectively. In the calculation, $\delta$ has been set to zero, since no mixing ratio could be deduced from the present data; the error introduced under this assumption is expected to be less than 10%.

The spin assignment for band 1 is proposed according to the systematics of $E_\gamma(7^+\to5^+)$ in the similar bands of $^{178-186}$Ir [25–28] (the configuration assignments will be discussed in the next section). The linking transitions of $E2$ character between band 1 and band 2 fix unambiguously the spin and parity of band 2 relative to band 1. The lowest level of band 3 is proposed to be $I_0^\pi=(8^-)$ based on level spacing systematics in the similar bands of neighboring odd-odd nuclei; this spin assignment leads to a consistent pattern of level staggering [5]. For the strongly coupled band 4, the lowest level is considered to be the bandhead with $I_0=K^+=\Omega_p+\Omega_n=9/2+7/2=8$. This spin assignment is further supported by the $B(M1;I\to I-1)/B(E2;I\to I-2)$ ratios and the signature splitting as discussed in the next section.

The relative intensities for some uncontaminated $\gamma$ rays could be measured in the total projection spectrum. Most of the values were extracted from the spectra gated on the bottom transitions in the band. Such a restriction means that the errors associated with relative intensities are often larger than those associated with the branching ratios, since the latter were obtained from a gate on the transitions above each state of interest. For some weak or heavily contaminated $\gamma$ rays, only upper or lower limits are given based on their intensity balance. The $\gamma$-ray energies, spin and parity assignments, relative $\gamma$-ray intensities, branching ratios, extracted $B(M1)/B(E2)$ values, and the DCO ratios are presented in Table I grouped in sequences for each band.

## III. DISCUSSION

### A. Preliminary remarks

The two-quasiparticle intrinsic states of an odd-odd nucleus can be well characterized by semiempirical calculations [4,29,30]. Such calculations have been performed for $^{180}$Ir with a simplified zero-order approximation [4] without taking the Gallagher-Moszkowski (GM) splitting [31] into account. The $\pi1/2^-[541]$, $\pi5/2^+[402]$, $\pi9/2^-[514]$, $\nu1/2^-[521]$, $\nu7/2^-[514]$, $\nu5/2^-[512]$, and $\nu9/2^+[624]$ intrinsic states have been observed at low energies in the neighboring $^{179,181}$Ir [21,22], $^{179}$Os [32–34], and $^{181}$Pt [35] nuclei. The calculated results for the related two-quasiparticle intrinsic states in $^{180}$Ir are displayed in Fig. 5 and referenced in the following configuration assignments.

For a rotational band, the in-band transition properties are sensitive to the quasiparticle configurations; thus they are often used as criteria for configuration assignments. In the framework of a rotational model, the reduced $M1$- and $E2$-transition probabilities can be calculated from the formulas of Bohr and Mottelson [36]:

$$\begin{aligned}B(M1,I\to I-1)&=\frac{3}{4\pi}\mu_N^2G_{KK}^2\langle IK10|I-1K\rangle^2\\&=\frac{3}{4\pi}\mu_N^2G_{KK}^2\frac{(I+K)(I-K)}{(2I+1)I}\end{aligned} \tag{3}$$

and

$$\begin{aligned}B(E2,I\to I-2)&=\frac{5}{16\pi}e^2Q_0^2\langle IK20|I-2K\rangle^2\\&=\frac{5}{16\pi}(eQ_0)^2\frac{3}{2}\\&\quad\times\frac{(I+K)(I-K)(I-1+K)(I-1-K)}{I(I-1)(2I-1)(2I+1)}.\end{aligned} \tag{4}$$

Combining Eqs. (3) and (4), one obtains the $B(M1)/B(E2)$ ratios expressed as

$$\frac{B(M1,I\to I-1)}{B(E2,I\to I-2)}=\frac{8}{5}\frac{G_{KK}^2}{Q_0^2}\frac{(2I-1)(I-1)}{(I-1+K)(I-1-K)}\left(\frac{\mu_N^2}{e^2b^2}\right). \tag{5}$$

As shown in Ref. [37], the parameter $G_{KK}$ is defined in odd-odd deformed nuclei by

$$G_{KK}=K(g_K-g_R)=\Omega_p(g_{\Omega_p}-g_R)+\Omega_n(g_{\Omega_n}-g_R), \tag{6}$$

where $g_{\Omega_p}$ ($g_{\Omega_n}$) and $\Omega_p$ ($\Omega_n$) represent the $g$ factor and the angular momentum projected on the symmetry axis for the proton (neutron) in the associated neighboring odd-mass nuclei. Also, $g_K$ is the effective gyromagnetic factor for the related two-quasiparticle configuration. The signs of $\Omega_p$ and $\Omega_n$ are taken as in the expression $K=\Omega_p+\Omega_n$ and the $g_{\Omega_p}$ ($g_{\Omega_n}$) can be calculated in the framework of the Nils-

TABLE I. $\gamma$-ray transition energies, spin and parity assignments, $\gamma$ intensities, branching ratios, DCO ratios, and extracted $B(M1)/B(E2)$ ratios in $^{180}$Ir.

| $E_\gamma$ (keV) [a] | $J_i^\pi \rightarrow J_f^\pi$ [b] | $I_\gamma$ [c] | $\lambda$ [d] | DCO ratio | $B(M1)/B(E2)$ [e] |
|---|---|---|---|---|---|
| Band 1 | | | | | |
| 164.0 | $(7^+)\rightarrow(5^+)$ | $\geqslant$520 | | 0.95(15) | |
| 290.5 | $(9^+)\rightarrow(7^+)$ | 350 | | 1.04(15) | |
| 393.3 | $(11^+)\rightarrow(9^+)$ | 230 | | 1.06(15) | |
| 481.0 | $(13^+)\rightarrow(11^+)$ | 180 | | 1.05(15) | |
| 548.0 | $(15^+)\rightarrow(13^+)$ | 180 | | 1.08(15) | |
| 530.0 | $(17^+)\rightarrow(15^+)$ | 70 | | 1.02(15) | |
| 495.5 | $(19^+)\rightarrow(17^+)$ | 58 | | 0.96(20) | |
| 619.0 | $(17^+)\rightarrow(15^+)$ | 60 | | | |
| Band 2 | | | | | |
| 82.5 | $(7^+)\rightarrow(6^+)$ | $\geqslant$217 | | | |
| 198.8 | $(8^+)\rightarrow(6^+)$ | $\geqslant$200 | | | |
| 115.8 | $(8^+)\rightarrow(7^+)$ | $\geqslant$160 | 1.16 | 0.55(10) | 0.13(4) |
| 261.0 | $(9^+)\rightarrow(7^+)$ | 205 | | 0.94(15) | |
| 145.0 | $(9^+)\rightarrow(8^+)$ | 150 | 1.41 | 0.47(10) | 0.20(6) |
| 327.0 | $(10^+)\rightarrow(8^+)$ | 516 | | 1.07(15) | |
| 182.0 | $(10^+)\rightarrow(9^+)$ | 67 | 6.06 | 0.52(10) | 0.07(2) |
| 383.5 | $(11^+)\rightarrow(9^+)$ | 382 | | 0.94(15) | |
| 201.5 | $(11^+)\rightarrow(10^+)$ | 61 | 6.30 | 0.50(10) | 0.12(4) |
| 433.3 | $(12^+)\rightarrow(10^+)$ | 512 | | 0.99(15) | |
| 231.8 | $(12^+)\rightarrow(11^+)$ | 71 | 8.71 | 0.52(10) | 0.09(3) |
| 477.2 | $(13^+)\rightarrow(11^+)$ | 530 | | 0.94(15) | |
| 245.3 | $(13^+)\rightarrow(12^+)$ | 40 | 9.5 | | 0.12(3) |
| 514.0 | $(14^+)\rightarrow(12^+)$ | 530 | | 0.97(15) | |
| 268.5 | $(14^+)\rightarrow(13^+)$ | 70 | 7.5 | | 0.17(8) |
| 543.8 | $(15^+)\rightarrow(13^+)$ | 450 | | 0.96(15) | |
| 275.3 | $(15^+)\rightarrow(14^+)$ | 45 | 9.90 | | 0.16(5) |
| 549.0 | $(16^+)\rightarrow(14^+)$ | 328 | | 1.02(15) | |
| 273.5 | $(16^+)\rightarrow(15^+)$ | 30 | 10.5 | | 0.16(5) |
| 608.0 | $(16^+)\rightarrow(14^+)$ | 150 | | 0.90(15) | |
| 539.0 | $(17^+)\rightarrow(15^+)$ | 256 | | 0.96(15) | |
| 265.5 | $(17^+)\rightarrow(16^+)$ | $\leqslant$50 | | | |
| 443.0 | $(18^+)\rightarrow(16^+)$ | 90 | | 0.92(20) | |
| 502.0 | $(18^+)\rightarrow(16^+)$ | 170 | | 1.00(15) | |
| 236.5 | $(18^+)\rightarrow(17^+)$ | $\leqslant$50 | | | |
| 497.5 | $(19^+)\rightarrow(17^+)$ | 104 | | 0.95(15) | |
| 260.5 | $(19^+)\rightarrow(18^+)$ | $\leqslant$50 | | | |
| 539.8 | $(20^+)\rightarrow(18^+)$ | 120 | | 0.92(15) | |
| 280.0 | $(20^+)\rightarrow(19^+)$ | $\leqslant$50 | | | |
| 570.0 | $(21^+)\rightarrow(19^+)$ | 80 | | 0.80(20) | |
| 590.3 | $(22^+)\rightarrow(20^+)$ | 120 | | 1.10(20) | |
| 641.5 | $(24^+)\rightarrow(22^+)$ | 60 | | 1.08(20) | |
| 695.3 | $(26^+)\rightarrow(24^+)$ | 50 | | | |
| Transitions | from 1 to 2 | | | | |
| 273.7 | $(9^+)\rightarrow(7^+)$ | 240 | | 0.95(15) | |
| Transitions | from 2 to 1 | | | | |
| 277.8 | $(9^+)\rightarrow(7^+)$ | | | 1.08(15) | |
| Band 3 | | | | | |
| 91.2 | $(9^-)\rightarrow(8^-)$ | $\geqslant$137 | | 1.45(50) | |
| 146.5 | $(10^-)\rightarrow(8^-)$ | $\geqslant$136 | | | |
| 55.3 | $(10^-)\rightarrow(9^-)$ | $\geqslant$250 | 0.40(10) | | 0.70(20) |
| 254.4 | $(11^-)\rightarrow(9^-)$ | $\geqslant$186 | | | |

TABLE I. (*Continued*).

| $E_\gamma$ (keV) [a] | $J_i^\pi \rightarrow J_f^\pi$ [b] | $I_\gamma$ [c] | $\lambda$ [d] | DCO ratio | $B(M1)/B(E2)$ [e] |
|---|---|---|---|---|---|
| 199.1 | $(11^-)\rightarrow(10^-)$ | $\geqslant 484$ | 0.38(10) | 0.50(8) | 0.25(7) |
| 285.1 | $(12^-)\rightarrow(10^-)$ | 524 | | 1.10(15) | |
| 85.5 | $(12^-)\rightarrow(11^-)$ | 100 | 5.8(1.7) | | 0.36(11) |
| 387.5 | $(13^-)\rightarrow(11^-)$ | $\leqslant 235$ | | | |
| 301.8 | $(13^-)\rightarrow(12^-)$ | $\leqslant 257$ | 0.89(20) | 0.48(7) | 0.26(7) |
| 420.5 | $(14^-)\rightarrow(12^-)$ | 1000 | | 1.02(15) | |
| 118.8 | $(14^-)\rightarrow(13^-)$ | 50 | 18(5) | | 0.30(8) |
| 491.2 | $(15^-)\rightarrow(13^-)$ | $\leqslant 178$ | | | |
| 372.3 | $(15^-)\rightarrow(14^-)$ | $\leqslant 164$ | 1.06(15) | 0.40(10) | 0.36(7) |
| 537.6 | $(16^-)\rightarrow(14^-)$ | 740 | | 1.03(15) | |
| 573.5 | $(17^-)\rightarrow(15^-)$ | $\leqslant 155$ | | | |
| 408.1 | $(17^-)\rightarrow(16^-)$ | $\leqslant 141$ | 1.53(30) | 0.40(6) | 0.42(9) |
| 631.8 | $(18^-)\rightarrow(16^-)$ | 538 | | 1.17(25) | |
| 644.0 | $(19^-)\rightarrow(17^-)$ | 220 | | | |
| 420.5 | $(19^-)\rightarrow(18^-)$ | | | | |
| 700.0 | $(20^-)\rightarrow(18^-)$ | 317 | | 0.92(25) | |
| 697.8 | $(21^-)\rightarrow(19^-)$ | 140 | | | |
| 418.0 | $(21^-)\rightarrow(20^-)$ | $\leqslant 10$ | | | |
| 736.8 | $(22^-)\rightarrow(20^-)$ | 155 | | | |
| 720.0 | $(23^-)\rightarrow(21^-)$ | 98 | | | |
| Band 4 | | | | | |
| 78.5 [f] | $(8^-)\rightarrow(7^+)$ | 375 | | 1.08(15) | |
| 95.3 | $(9^-)\rightarrow(8^-)$ | 114 | | | |
| 131.0 | $(10^-)\rightarrow(9^-)$ | 130 | | 1.80(50) | |
| 287.5 | $(11^-)\rightarrow(9^-)$ | 45 | | 1.31(20) | |
| 156.4 | $(11^-)\rightarrow(10^-)$ | 223 | 0.19(3) | 1.20(15) | 1.88(37) |
| 343.8 | $(12^-)\rightarrow(10^-)$ | 180 | | 1.06(20) | |
| 187.3 | $(12^-)\rightarrow(11^-)$ | 247 | 0.50(8) | 1.20(20) | 1.02(20) |
| 397.8 | $(13^-)\rightarrow(11^-)$ | 174 | | 1.01(15) | |
| 210.3 | $(13^-)\rightarrow(12^-)$ | 218 | 0.86(12) | 1.24(20) | 0.87(17) |
| 440.8 | $(14^-)\rightarrow(12^-)$ | 213 | | 1.10(20) | |
| 230.3 | $(14^-)\rightarrow(13^-)$ | 170 | 1.41(21) | 1.13(20) | 0.67(13) |
| 477.9 | $(15^-)\rightarrow(13^-)$ | 273 | | 1.05(15) | |
| 247.5 | $(15^-)\rightarrow(14^-)$ | 145 | 2.07(30) | 1.24(20) | 0.55(11) |
| 510.0 | $(16^-)\rightarrow(14^-)$ | 268 | | 1.00(15) | |
| 262.3 | $(16^-)\rightarrow(15^-)$ | 89 | 2.86(45) | 1.23(20) | 0.47(9) |
| 539.3 | $(17^-)\rightarrow(15^-)$ | 248 | | 1.00(15) | |
| 277.0 | $(17^-)\rightarrow(16^-)$ | 80 | 3.46(60) | 1.30(20) | 0.43(10) |
| 566.8 | $(18^-)\rightarrow(16^-)$ | 220 | | 1.06(15) | |
| 289.8 | $(18^-)\rightarrow(17^-)$ | 68 | 3.46(60) | 1.43(40) | 0.48(10) |
| 594.1 | $(19^-)\rightarrow(17^-)$ | 200 | | 1.00(20) | |
| 304.3 | $(19^-)\rightarrow(18^-)$ | 56 | 5.1(1.0) | | 0.36(8) |
| 621.4 | $(20^-)\rightarrow(18^-)$ | 160 | | 0.93(20) | |
| 317.3 | $(20^-)\rightarrow(19^-)$ | 43 | 4.5(1.2) | | 0.45(13) |
| 649.3 | $(21^-)\rightarrow(19^-)$ | 157 | | | |
| 332.0 | $(21^-)\rightarrow(20^-)$ | 36 | 5.3(1.2) | | 0.42(12) |
| 678.8 | $(22^-)\rightarrow(20^-)$ | 89 | | | |
| 346.8 | $(22^-)\rightarrow(21^-)$ | 40 | 2.0(1.0) | | 1.20(60) |
| 704.5 | $(23^-)\rightarrow(21^-)$ | 128 | | | |
| 730.0 | $(24^-)\rightarrow(22^-)$ | $\leqslant 40$ | | | |
| 751.3 | $(25^-)\rightarrow(23^-)$ | $\leqslant 40$ | | | |

TABLE I. (*Continued*).

| $E_\gamma$ (keV) [a] | $J_i^\pi \rightarrow J_f^\pi$ [b] | $I_\gamma$ [c] | λ [d] | DCO ratio | $B(M1)/B(E2)$ [e] |
|---|---|---|---|---|---|
| Band 5 | | | | | |
| 147.1 | $I_0+1 \rightarrow I_0$ | 125 | | 1.68(50) | |
| 315.5 | $I_0+2 \rightarrow I_0$ | 80 | | | |
| 168.3 | $I_0+2 \rightarrow I_0+1$ | 218 | 0.37(11) | 1.13(20) | 1.23(37) |
| 354.8 | $I_0+3 \rightarrow I_0+1$ | 115 | | 1.00(20) | |
| 186.0 | $I_0+3 \rightarrow I_0+2$ | 180 | 0.69(20) | 1.08(30) | 0.88(26) |
| 386.0 | $I_0+4 \rightarrow I_0+2$ | 150 | | 0.88(20) | |
| 200.3 | $I_0+4 \rightarrow I_0+3$ | 140 | 1.04(31) | 1.28(20) | 0.72(22) |
| 413.8 | $I_0+5 \rightarrow I_0+3$ | 190 | | 1.10(20) | |
| 213.5 | $I_0+5 \rightarrow I_0+4$ | 105 | 1.82(54) | 1.30(30) | 0.48(14) |
| 440.3 | $I_0+6 \rightarrow I_0+4$ | 210 | | 1.05(20) | |
| 226.5 | $I_0+6 \rightarrow I_0+5$ | 85 | 2.44(73) | 1.30(40) | 0.40(12) |
| 466.5 | $I_0+7 \rightarrow I_0+5$ | 237 | | 1.02(20) | |
| 240.0 | $I_0+7 \rightarrow I_0+6$ | 76 | 3.3(1.0) | 1.60(50) | 0.34(10) |
| 492.3 | $I_0+8 \rightarrow I_0+6$ | 210 | | 1.10(20) | |
| 252.3 | $I_0+8 \rightarrow I_0+7$ | 55 | 3.8(1.1) | | 0.33(10) |
| 519.0 | $I_0+9 \rightarrow I_0+7$ | 202 | | 0.87(20) | |
| 266.5 | $I_0+9 \rightarrow I_0+8$ | 40 | 3.3(1.0) | | 0.42(13) |
| 544.8 | $I_0+10 \rightarrow I_0+8$ | 146 | | 1.08(20) | |
| 278.2 | $I_0+10 \rightarrow I_0+9$ | 30 | 4.0(1.5) | | 0.39(15) |
| 564.5 | $I_0+11 \rightarrow I_0+9$ | 150 | | 0.91(25) | |
| 586.5 | $I_0+12 \rightarrow I_0+9$ | 120 | | 1.10(25) | |
| 622.3 | $I_0+13 \rightarrow I_0+11$ | 123 | | | |
| 634.0 | $I_0+14 \rightarrow I_0+12$ | 101 | | | |
| 653.3 | $I_0+15 \rightarrow I_0+13$ | 78 | | | |

[a]Uncertainties between 0.1 and 0.5 keV.
[b]See text for details about the spin and parity assignments.
[c]Uncertainties between 5% and 30%.
[d]Branching ratio: $T_\gamma(I \rightarrow I-2)/T_\gamma(I \rightarrow I-1)$, $T_\gamma(I \rightarrow I-2)$ and $T_\gamma(I \rightarrow I-1)$ are the relative $\gamma$ intensities of the $E2$ and $M1$ transition depopulating the level $I$, respectively.
[e]Extracted from the branching ratios assuming $\delta^2=0$.
[f]$\gamma$-ray deexcitating the bandhead.

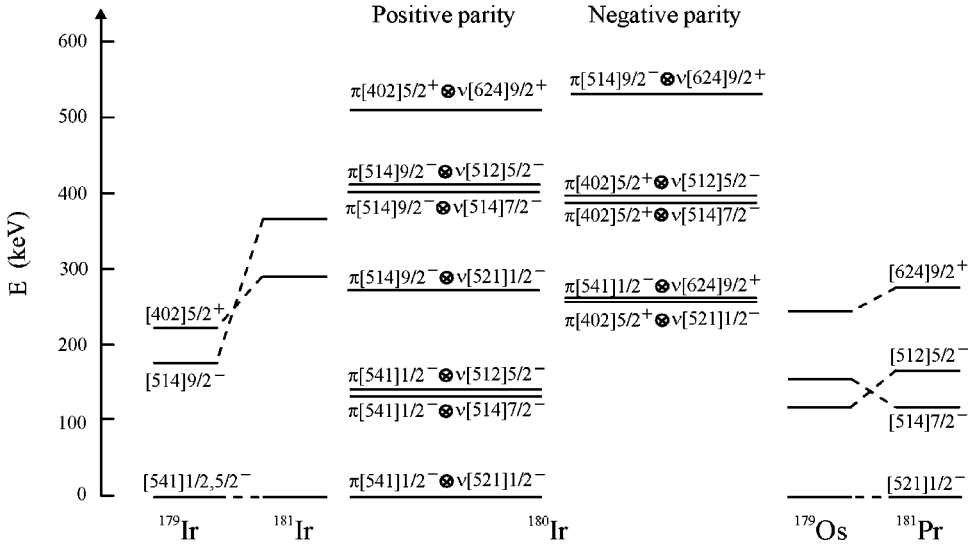


FIG. 5. Predicted bandhead excitation energies in $^{180}$Ir based on the zero-order approximation of Ref. [4].

TABLE II. Possible configurations for bands in $^{180}$Ir and their $g_K$ factors calculated using Eq. (6). Here $g_{\Omega p}$ and $g_{\Omega n}$ values are taken from Ref. [4].

| | | $p_{3/2}$ $1/2^-[521]$ $g_{\Omega n}=0.697$ | $h_{9/2}$ $5/2^-[512]$ $g_{\Omega n}=-0.31$ | $i_{13/2}$ $7/2^+[633]$ $g_{\Omega n}=-0.253$ | $f_{7/2}$ $7/2^-[514]$ $g_{\Omega n}=0.33$ | $i_{13/2}$ $9/2^+[624]$ $g_{\Omega n}=-0.30$ |
|---|---|---|---|---|---|---|
| $h_{9/2}$-$1/2^-[541]$ | $K^\pi$; $g_K$ | $1^+$, 0.76 | $3^+$; $-0.12$ | $4^-$; $-0.12$ | $4^+$; 0.39 | $5^-$; 0.04 |
| $g_{\Omega p}=0.83$ | | – | $2^+$; $-0.60$ | $3^-$; $-0.43$ | $3^+$ ; 0.25 | $4^-$; $-0.75$ |
| $h_{11/2}$-$9/2^-[514]$ | $K^\pi$; $g_K$ | $5^+$; 1.23 | $7^+$; 0.72 | $8^-$; 0.61 | $8^+$; 0.87 | $9^-$; 0.50 |
| $g_{\Omega p}=1.29$ | | $4^+$; 1.36 | $2^+$; 3.29 | $1^-$; 5.14 | $1^+$; 4.65 | – |
| $d_{5/2}$-$5/2^+[402]$ | $K^\pi$; $g_K$ | $3^-$; 1.43 | $5^-$; 0.63 | $6^+$; 0.51 | $6^-$; 0.85 | $7^+$; 0.37 |
| $g_{\Omega p}=1.57$ | | $2^-$; 1.79 | – | $1^+$; $-4.81$ | $1^-$; $-2.77$ | $2^+$; $-2.64$ |

son model. The calculated results can be found in Ref. [4] and are used here to calculate $g_K$ according to Eq. (6). The calculated $g_K$ values are given in Table II for different two-quasiparticle configurations. The $Q_0$ is the intrinsic quadrupole moment of the nucleus. We choose $Q_0=6.5(e\,\mathrm{b})$ which is a reasonable value for the ground-state bands in even-even neighbors [38]. The collective $g$ factors are taken as $g_R=0.30$ for variant quasiparticle configurations. From Eq. (5), the $B(M1)/B(E2)$ ratios have been calculated for various possible configurations, and these results were compared with experiment. Reasonable agreement between theory and experimental data is taken to be a supplementary argument for configuration assignments.

Because the five rotational bands observed in this work are ''floating'' in energy, it is difficult to determine the spin and parity of the levels with conventional spectroscopic methods. This leads to uncertainty in the configuration assignments. Therefore we utilize different criteria in determining quasiparticle configurations, such as predicted bandhead energies, band structure systematics, alignments, band crossing frequencies, $B(M1)/B(E2)$ ratios, signature splitting, etc. These structural properties will be addressed in the following sections.

### B. Band 1

Band 1 has been reported previously [19] and was considered to be the doubly decoupled band based on the $\pi 1/2^-[541]\otimes\nu 1/2^-[521]$ configuration. We have assigned two new transitions (495.5- and 530.0-keV lines) to this band, thus extending it up to $(19^+)$. Several arguments support this configuration assignment. First, the predicted bandhead is the lowest one as shown in Fig. 5. Second, the measured DCO ratios (see Table I) for the related $\gamma$ rays indicate that these transitions have stretched $E2$ characteristics. A careful evaluation of the intensity balance leads to a consistent interpretation only if $E2$ multipolarity is assumed for the 164-keV transition in band 1, given the large difference in internal conversion for low-energy $M1$, $E1$, and $E2$ transitions. Third, the general conditions for double decoupling have been theoretically investigated in odd-odd iridium and rhenium isotopes, and the observation of such a doubly decoupled band in $^{180}$Ir is consistent with theoretical expectations [27,28]. Finally, excitation energies in the doubly decoupled bands of $^{178-186}$Ir [25,27,28] built on the $(5^+)$ state are compared in Fig. 6. Good systematics in level spacings support the configuration assignment cited above and the spin and parity for the lowest level is thus suggested to be $(5^+)$.

From a closer inspection of Fig. 6 one can find that the excitation energies change smoothly as a function of the number of neutron pairs for the first two excited states. This smooth variation is apparently associated with the similar behavior of low-lying levels in the ground-state bands of their even-even cores and could be understood as the smooth change of masses and deformations. However, for the levels above $(11^+)$, a striking staggering of the levels appears. This staggering has not yet been understood and needs a full explanation.

### C. Band 2

The odd-spin sequence of band 2 has been extended from $(17^+)$ up to $(21^+)$ by adding two cascade $\gamma$ rays (497- and 570-keV lines) to the previous results [19]. Two linking transitions (273.7 and 277.8 keV) between band 1 and 2 are clearly identified and shown in Figs. 3(a) and 3(b). Such strong linking transitions can be understood if we assumed that two states of equal $I^\pi$ come so close in energy that they mix significantly. Their DCO ratios are measured to be 0.95(10) and 1.08(10), respectively. Comparing with the DCO ratios of in-band $\Delta I=1$ transitions [e.g., 0.47(10) and 0.55(10) for the 145- and 115.8-keV lines in band 2], the linking transitions are considered to be stretched $E2$ transitions. These connections fix unambiguously the spin and parity of band 2 relative to band 1, as shown in Fig. 2. It is worthwhile to note that a band with similar linking transitions to the doubly decoupled one at $(9^+)$ has been identified in $^{182}$Ir but assigned to the $\pi 5/2^+[402]\otimes\nu i_{13/2}$ configuration [26]. In Fig. 7 we plot the alignments $i_x$ and the dynamical moments of inertia, $J^{(2)}$, versus rotational frequency $\hbar\omega$. A sudden upbend is clearly observed at $\hbar\omega_c=0.26$ MeV. This band crossing frequency is very close to the value of $\hbar\omega_c=0.25(1)$ MeV in the $\nu 5/2^-[512]$ band of $^{179}$Os [32,33] but smaller than $\hbar\omega_c=0.30$ MeV in the yrast band of $^{178}$Os [39,40]. The alignment gain at the band crossing is

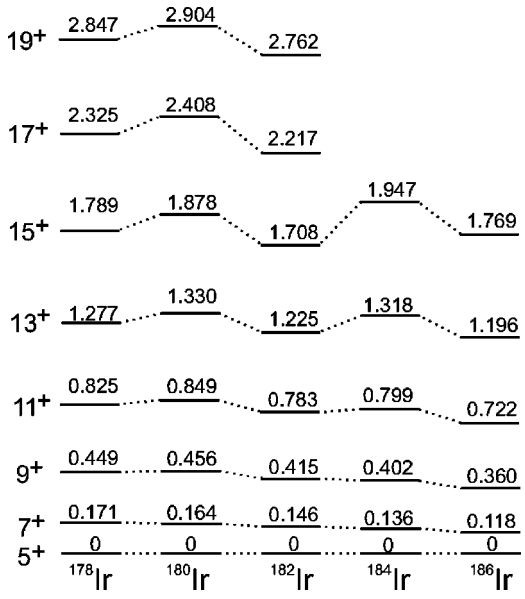


FIG. 6. Level spacing systematics for the doubly decoupled bands in $^{178}$Ir [25], $^{180}$Ir (this work), $^{182}$Ir [27], $^{184}$Ir [27], and $^{186}$Ir [28].

about $7\hbar$, which is consistent with that in the $\pi 1/2^-[541]$ band of $^{179}$Ir [21], corresponding to alignment of the first pair of $i_{13/2}$ neutrons. Thus, the band crossing of band 2 can be explained [1,41] as being due to the neutron $AB$ crossing expected in the framework of the cranked shell model. The observation of band crossing at $\hbar\omega_c = 0.26$ MeV excludes the participation of a $i_{13/2}$ neutron for this structure according to the blocking arguments. Therefore, the most probable configurations for this band would be $\pi 1/2^-[541] \otimes \nu 5/2^-[512]$ or $\pi 1/2^-[541] \otimes \nu 7/2^-[514]$ as expected from the predicted bandhead energies shown in Fig. 5. We have also compared the experimental $B(M1;I \rightarrow I-1)/B(E2;I \rightarrow I-2)$ ratios, extracted from the in-band branching ratios, to the theoretical predictions from Eq. (5). The experimental and the calculated results are presented in Fig. 8(a) from which one may conclude that the assignment of the $\pi 1/2^-[541] \otimes \nu 5/2^-[512]$ configuration is the most probable.

For the deformed rare-earth nuclei, the occupation of the $1/2^-[541]$ intruder orbital by a quasiproton is usually considered to drive the nucleus to a larger quadrupole deformation and lead to a delayed band crossing frequency [42]. For example, the neutron $AB$ crossing frequency $\hbar\omega_c(AB)$ in the $\pi 1/2^-[541]$ band of $^{175}$Ta has been deduced [43] to be 75 keV delayed with respect to that in the yrast band of neighboring even-even nuclei. The very similar $AB$ crossing frequencies, both in the $\pi 1/2^-[541] \otimes \nu 5/2^-[512]$ band of $^{180}$Ir and in the $\nu 5/2^-[512]$ band of $^{179}$Os, indicate that the shape driving effects of the $\pi 1/2^-[541]$ intruder orbital might be negligible or very small for iridium isotopes. With this in mind, we consider that the $AB$ crossing frequency in $^{178}$Os should be close to that in the $\pi 1/2^-[541]$ band of $^{179}$Ir. This is supported by Refs. [21,39,40], which show that the $\hbar\omega_c(AB)$ values are almost the same for both the $\pi 1/2^-[541]$ band in $^{179}$Ir and the yrast band in $^{178}$Os. The

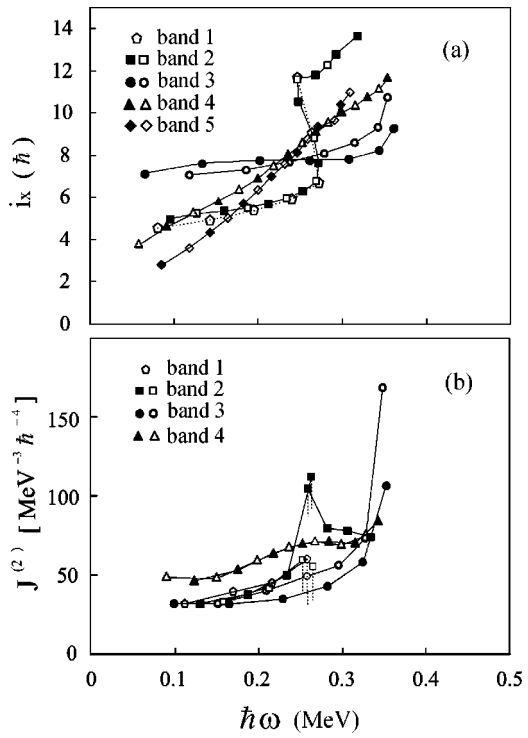


FIG. 7. Quasiparticle alignments $i_x$ and dynamical moments of inertia, $J^{(2)}$, as a function of rotational frequency for the four bands in $^{180}$Ir. The common Harris parameters are taken to be $J_0 = 23$ MeV$^{-1}\hbar^2$, $J_1 = 75$ MeV$^{-3}\hbar^4$ in order that band 3 has roughly constant alignment before the band crossing; $I_0 = K^+ = 7$ is used for band 5.

smaller $AB$ crossing frequencies in the $\nu 1/2^-[521]$, $\nu 5/2^-[512]$, $\pi 1/2^-[541] \otimes \nu 1/2^-[521]$ and $\pi 1/2^-[541] \otimes \nu 5/2^-[512]$ bands are caused by blocking effects, in that the neutron pairing $\Delta_n$ is reduced when the $\nu 1/2^-[521]$ or $\nu 5/2^-[512]$ orbital is occupied. As a consequence, the alignment of the first pair of $i_{13/2}$ neutrons may occur at a lower rotational frequency.

### D. Band 3

Band 3 has been reported in our previous publication [19] where the quasiparticle configuration of $\pi 1/2^-[541](\alpha = 1/2) \otimes \nu i_{13/2}(\alpha = \pm 1/2)$ has been proposed. The deduced experimental $B(M1)/B(E2)$ ratios versus spin $I$ are plotted and compared with theoretical predictions in Fig. 8(b). The agreement is rather good under the assumption of this configuration. The spin assignment and low-spin signature inversion were already discussed in Ref. [19]. In this paper, we concentrate on its quasiparticle alignments and band crossings in comparison with those of the neighboring nuclei.

Figure 7 shows the plots of quasiparticle alignments $i_x(\omega)$ and dynamic moments of inertia, $J^{(2)}(\omega)$, versus the rotational frequency $\hbar\omega$ for all the bands observed. The band crossing seems to occur at about $\hbar\omega_c \sim 0.35$ MeV for band 3, which is consistent with the expectations in Ref. [1]. It is noted that the alignments of two $\Delta I = 2$ signature branches cross at a certain frequency when the common Harris parameters are used. This feature has been found in the

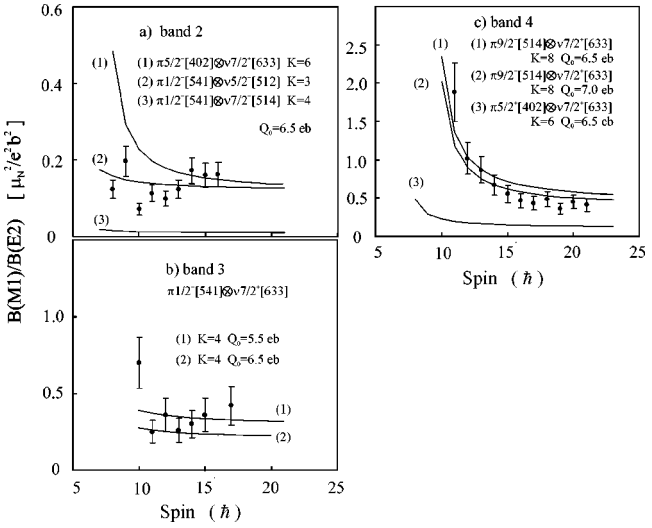


FIG. 8. Experimental $B(M1)/B(E2)$ ratios and theoretical predictions under the assumption of various configurations as indicated in the figure.

$\nu i_{13/2}$ bands of $^{179}$Os and $^{183}$Pt [32,44] and has been attributed to signature-dependent deformations.

If the shape driving effects of the $\pi 1/2^-[541]$ intruder orbital are negligible and have no obvious influence on band crossing frequencies (see discussions in the preceding subsection), one may expect that the neutron $BC$ crossing in both the $\nu i_{13/2}$ band of $^{179}$Os and the $\pi 1/2^-[541]\otimes\nu i_{13/2}$ band of $^{180}$Ir should occur at a similar frequency, larger than the neutron $AB$ crossing frequency of $\hbar\omega_c(AB)=0.300(5)$ MeV in the yrast band of $^{178}$Os. However, the neutron $BC$ crossing frequency is extracted to be $\hbar\omega_c(BC)=0.305(5)$ MeV in the $\nu i_{13/2}$ band of $^{179}$Os, whereas no clear band crossing is observed in the $\pi 1/2^-[541]\otimes\nu i_{13/2}$ band up to $\hbar\omega\sim 0.34$ MeV. To understand this phenomenon, we refer to the theoretical work reported in Refs. [12,14,21,44–46]. The neutron Fermi surface lies between the $\nu 7/2^+[633]$ and $\nu 9/2^+[624]$ orbitals for the $N=103$ nucleus $^{179}$Os. The TRS calculations have shown that such a $i_{13/2}$ quasineutron drives the nucleus from axially symmetric to a triaxial shape with slightly smaller $\beta_2$ and larger negative $\gamma$ up to $-14°$ [44], leading to the reduced neutron $BC$ and $AD$ crossings. This could be the reason that $\hbar\omega_c(BC)$ in $^{179}$Os is close to $\hbar\omega_c(AB)$ in $^{178}$Os. The theoretical calculations predict (see, for example, Ref. [14]) that the nucleus has roughly constant deformations of $\beta_2\sim 0.23$ and $\gamma\geqslant 0°$ when the proton intruder orbital $1/2^-[541]$ is occupied. Therefore, the $\hbar\omega_c(BC)$ and $\hbar\omega_c(AD)$ in the $\pi 1/2^-[541]\otimes\nu i_{13/2}$ band of $^{180}$Ir become larger than that in the $\nu i_{13/2}$ band of $^{179}$Os. The stabilization effects of $1/2^-[541]$ proton excitation are reflected by the decreasing signature splitting in the $\pi 1/2^-[541]\otimes\nu i_{13/2}$ band of $^{180}$Ir as compared to the signature splitting in the $\nu i_{13/2}$ band of $^{179}$Os. In fact, the signature splitting in both bands originate from the $i_{13/2}$ neutron. A large negative $\gamma$ caused by the $i_{13/2}$ neutron leads to an enhanced signature splitting [44], whereas the $1/2^-[541]$ proton stabilizes the nucleus against $\gamma$ deformation. Consequently, the signature splitting becomes smaller in the $\pi 1/2^-[541]\otimes\nu i_{13/2}$ two-quasiparticle band.

### E. Strongly coupled bands 4 and 5

Band 4 is newly identified. It shows the strongly coupled characters of intense in-band $M1/E2$ transitions [see Figs. 2 and 4(b)] and small signature splittings. The strong $M1/E2$ transitions indicate a high-$K$ and/or a large-$g_K$ factor involved in this structure. Considering all the possible low-lying intrinsic states shown in Fig. 5, we suggest that the configuration $\pi 9/2^-[514](\alpha=\pm 1/2)\otimes\nu i_{13/2}(\alpha=+1/2)$ (with $\nu 7/2^+[633]$ as the main component) should be the best candidate. The experimental $B(M1)/B(E2)$ ratios have been deduced and compared with theoretical calculations in Fig. 8(c). The calculated result for the $\pi 5/2^+[402](\alpha=\pm 1/2)\otimes\nu i_{13/2}(\alpha=+1/2)$ configuration is also presented since such a configuration also has a large-$g_K$ factor (see Table II) and gives rise to a strongly coupled structure. One can see in this figure that the experimental $B(M1)/B(E2)$ ratios are fairly well reproduced if the configuration $\pi 9/2^-[514]\otimes\nu i_{13/2}$ is assumed. In fact, the proton $h_{11/2}$-$9/2^-[514]$ bands in $^{179}$Ir and $^{181}$Ir have been observed to be low-lying and intensely populated in the heavy-ion-induced fusion-evaporation reactions [21,22]. The neutron $i_{13/2}$ bands are yrast in the neighboring odd-$N$ nuclei. Consequently the two-quasiparticle band based on the $\pi 9/2^-[514]\otimes\nu i_{13/2}$ configuration is expected to be easily populated in the (HI,$xn$) reaction used in this experiment. The similar strongly coupled bands have been identified in the neighboring odd-odd $^{174}$Ta [10], $^{174-178}$Re [47,4,48], and $^{178}$Ir [5] nuclei.

The spin assignment for band 4 has been proposed on the basis of level spacing systematics in the similar bands of neighboring odd-odd nuclei; this method has been applied previously to the odd-odd nuclei in the $A=130,160$ mass region and it fixes the level spins within $1\hbar$ [49,50]. The relative excitation energies, normalized to $(9^-)$ levels, are shown in Fig. 9 for the favored (signature $\alpha=1$) $\Delta I=2$ transition sequences in the $\pi 9/2^-[514]\otimes\nu i_{13/2}$ bands of $^{180}$Ir together with those of $^{174}$Ta [10], $^{174-178}$Re [47,4,48], and $^{178}$Ir [5]. Note that the spin assignment for $^{178}$Re is increased by one unit with respect to the original one [48] and is consistent with the suggestion in Refs. [4,11]. The spin assignment for $^{174}$Re was not given in our previous publication [47]. From this figure, one may find that the level energies of band 4 in $^{180}$Ir fit well with the systematics if the proposed $I^\pi$ values are accepted. The level spacing systematics also support the spin assignment for the $\pi 9/2^-[514]\otimes\nu i_{13/2}$ bands in $^{174}$Re as shown in Fig. 9. The satisfactory agreement between the calculated and experimental $B(M1)/B(E2)$ ratios can be regarded, in turn, as a supplementary support to the spin assignment.

It should be noted that $\nu i_{13/2}$-$9/2^+[624]$ is closer to the neutron Fermi surface than $\nu i_{13/2}-7/2^+[633]$ in the odd-mass Os isotopes with $N\geqslant 105$; this ordering is reversed for isotopes with $N\leqslant 101$. For the $N=103$ isotones, both orbitals may be equally close to the Fermi surface. The strongly Coriolis-mixed bands in $^{179}$Os and $^{181}$Pt have been assigned to the $\nu i_{13/2}$-$9/2^+[624]$ configuration [32–35]. However, the

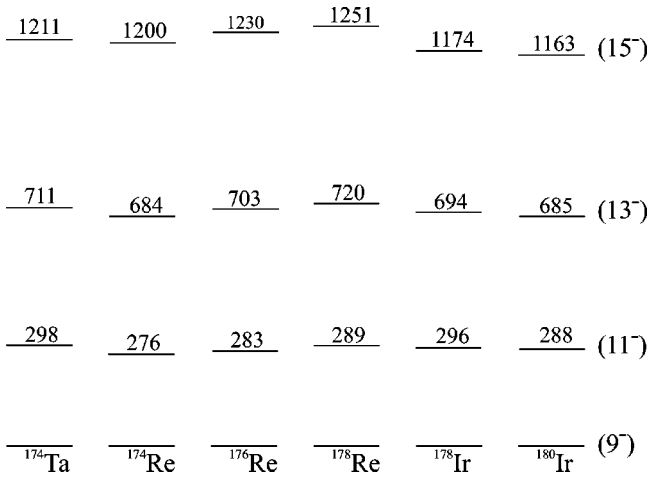


FIG. 9. Level spacing systematics for the $\pi h_{11/2}\otimes \nu i_{13/2}$ strongly coupled bands in $^{174}$Ta [10], $^{174-178}$Re [47,4,48], $^{178}$Ir [5], and $^{180}$Ir (this work).

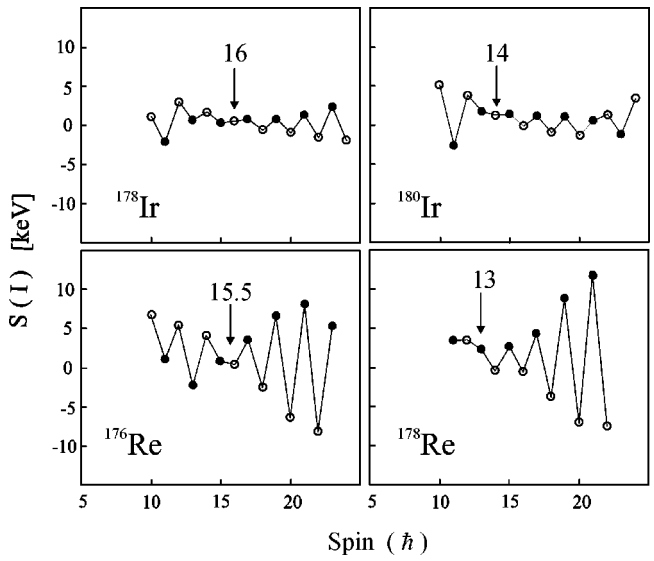


FIG. 10. Signature splitting $S(I)$ as a function of spin $I$ for the $\pi h_{11/2}\otimes \nu i_{13/2}$ strongly coupled bands in $^{178}$Ir [5]. $^{180}$Ir (this work), $^{176}$Re [4], and $^{178}$Re [4,48].

cranked shell model calculations performed in our laboratory and in Ref. [41] have shown that $\nu i_{13/2}$-7/2$^+$[633] is closer to the Fermi surface than $\nu i_{13/2}$-9/2$^+$[624]. Therefore, $\nu i_{13/2}$-7/2$^+$[633] is suggested to be the main component in band 4 of $^{180}$Ir, leading to a reasonable bandhead spin of $I_0=K^+=\Omega_p+\Omega_n=9/2+7/2=8$. This spin assignment is further supported by the pattern of signature splitting, $S(I)$, defined as

$$S(I)=[E(I)-E(I-1)]-\frac{1}{2}[E(I+1)-E(I)+E(I-1)-E(I-2)]. \quad (7)$$

Here $E(I)$ is the level energy of state $I$; $S(I)$ is directly proportional to the energy difference of the two signatures, but magnified by approximately a factor of 2. The plot of $S(I)$ versus $I$ for band 4 is compared in Fig. 10 with those for the $\pi 9/2^-[514]\otimes \nu i_{13/2}$ bands in $^{178}$Ir [5] and $^{176,178}$Re [4,11,48]. It can be seen that the staggering phase of band 4 in $^{180}$Ir is the same as that in the $\pi 9/2^-[514]\otimes \nu i_{13/2}$ bands of $^{178}$Ir and $^{176,178}$Re. In particular, all the $\pi 9/2^-[514]\otimes \nu i_{13/2}$ bands feature low-spin signature inversion. This is a systematic behavior for the $\pi h_{11/2}\otimes \nu i_{13/2}$ bands in lighter odd-odd nuclei in this mass region. Note that the linking transitions have been established between the $\pi 9/2^-[514]\otimes \nu i_{13/2}$ and $\pi 1/2^-[541]\otimes \nu i_{13/2}$ bands in $^{176,178}$Re [4,48]. These linking transitions lead to unambiguous spin and parity assignments of one band relative to the other. In Refs. [4,11], bandhead spins for the $\pi 9/2^-[514]\otimes \nu i_{13/2}$ bands in $^{176,178}$Re were proposed to be $(8^-)$. If the bandhead spin is assigned to be $(9^-)$ in $^{180}$Ir (formed by coupling a 9/2$^-$[514] proton with a 9/2$^+$[624] neutron), the phase of level staggering for band 4 would be opposite to those of similar bands in the neighboring $^{178}$Ir and $^{176,178}$Re nuclei.

In addition to band 4, another weakly populated band (labeled as band 5 in Fig. 3) has been identified and assigned to $^{180}$Ir. This is a strongly coupled band characterized by intense in-band $M1/E2$ transitions and small signature splittings. The extracted in-band $B(M1)/B(E2)$ ratios are comparable with those of band 4 (see Table I). Considering the calculated zero-order level scheme shown in Fig. 5, we associate band 5 with $\pi 5/2^+[402]\otimes \nu 9/2^+[624]$ or $\pi 9/2^-[514]\otimes \nu 9/2^+[624]$ since both configurations have high-$K$ and large-$g_K$ factors (see Table II). The deduced $B(M1)/B(E2)$ ratios are compared with theoretical predictions in Fig. 11 under the assumption of various configurations. One can find in Fig. 11 (a) that the experimental $B(M1)/B(E2)$ ratios can be very well reproduced if the $\pi 9/2^-[514]\otimes \nu 9/2^+[624]$ configuration with bandhead spin of $I_0=K^+=\Omega_p+\Omega_n=9/2+9/2=9$ is assumed. If the same procedure is applied to the $\pi 5/2^+[402]\otimes \nu 9/2^+[624]$ configuration with $I_0=K^+=\Omega_p+\Omega_n=5/2+9/2=7$ and a common collective $g$ factor of $g_R=0.3$, then the calculated $B(M1)/B(E2)$ ratios are systematically smaller than the experimental ones [see Fig. 11(b)]. However, if a reasonable $g_R=0.24$ is used instead of 0.3, the experimental $B(M1)/B(E2)$ ratios can be well fitted by the calculations as shown in Fig. 11(b); therefore further investigation is needed for the configuration assignment of band 5.

Finally, we would like to point out that the deduced DCO ratios for the $\Delta I=1$ in-band transitions in bands 4 and 5 all deviate from 0.6; in most cases the $R_{DCO}(\gamma)$ values are close to or larger than unity (see Table I). This may be understood if a positive sign is assumed for $\delta$ in these $\Delta I=1$ in-band transitions. In fact, $\delta=+0.31$ was estimated for the $(11^-)\rightarrow(10^-)$ transition in the $\pi 9/2^-[514]\otimes \nu 7/2^+[633]$ band of $^{176}$Re [4].

### F. Gradual alignment gain in band 4

In Fig. 7(a), one can see that the first three bands behave normally, with roughly constant alignment at lower frequencies up to a sudden increase at backbends; this is expected when the intruder orbital $\pi 1/2^-[541]$ is occupied. However,

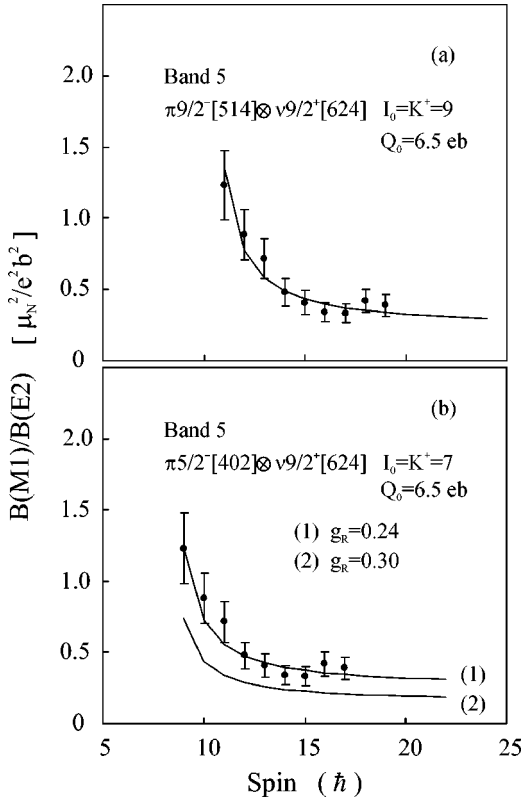


FIG. 11. Experimental $B(M1)/B(E2)$ ratios for band 5 and theoretical predictions under the assumption of different configurations as indicated on the panels.

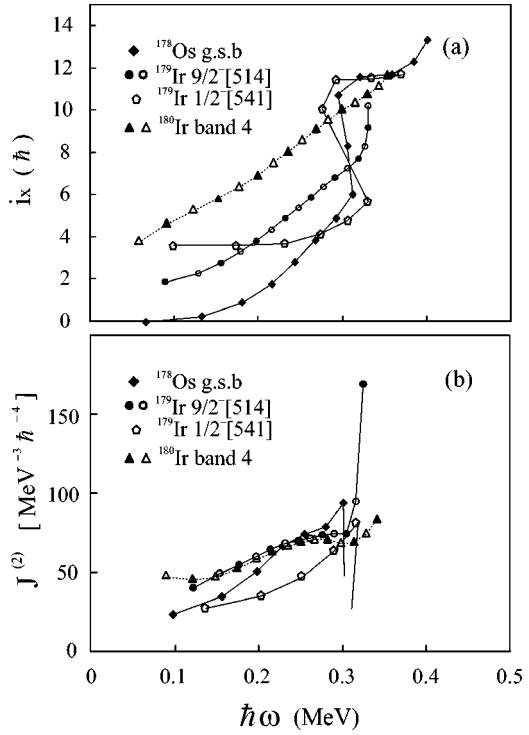


FIG. 12. Quasiparticle alignments $i_x$ and dynamical moments of inertia, $J^{(2)}$, as a function of rotational frequency for band 4 in $^{180}$Ir, the ground-state band in $^{178}$Os [39], and the $\pi 1/2^-[541]$ and $\pi 9/2^-[514]$ bands in $^{179}$Ir [21]. We used the same common Harris parameters as in Fig. 7.

band 4 shows considerable alignment gain from $\sim 4\hbar$ at low rotational frequency up to $\sim 12\hbar$ at the highest measured frequency; no backbend has been observed. A similar alignment pattern has also been observed in band 5. To further confirm such an anomalous alignment in odd-odd $^{180}$Ir, we give the dynamic moments of inertia, $J^{(2)}$, versus the rotational frequency $\hbar\omega$ in Fig. 7(b) for the observed four bands. Such plots are insensitive to the spin assignment since $J^{(2)}$ $(\hbar\omega)$ equals $\sim 4/\Delta E_\gamma(I)$ and can be calculated directly from observed $\gamma$-ray energies, $E_\gamma(I)$. The dotted line in Fig. 7 (b) indicates a sharp discontinuity at that point corresponding to the first backbend. One can observe an interesting feature in that the $J^{(2)}$ for band 4 shows a broad shoulder (or bump) at rotational frequencies before backbending, whereas this shoulder disappears for the bands with $\pi 1/2^-[541]$ occupied. Apparently the shoulder in the $J^{(2)}$ vs $\hbar\omega$ plots is related to the gradual alignment gain in the $i_x$ vs $\hbar\omega$ plots.

Figure 12 presents the plots of $i_x$ and $J^{(2)}$ vs $\hbar\omega$ for the yrast band in $^{178}$Os [39], the $\pi 9/2^-[514]$ and $\pi 1/2^-[541]$ bands in $^{179}$Ir [21], and band 4 in $^{180}$Ir. The gradual alignment gains and broad shoulders in the $J^{(2)}$ vs $\hbar\omega$ plots are observed in similar frequency ranges for the yrast band in $^{178}$Os and the $\pi 9/2^-[514]$ band in $^{179}$Ir; such phenomena have disappeared in the $\pi 1/2^-[541]$ decoupled band. Considering the striking similarity to band 4 in $^{180}$Ir, one may conclude that the low-frequency anomalies both in $J^{(2)}$ and in $i_x$ observed in band 4 are closely related to those in the yrast band of $^{178}$Os and the $\pi 9/2^-[514]$ band of $^{179}$Ir; they may originate from the same physical reasons. Note that the gradual alignment gain has been observed in the ground-state bands of even-even Os and Pt neighbors and in the $\pi 5/2^+[402]$ and $\pi 9/2^-[514]$ bands of neighboring odd-$Z$ nuclei (see Ref. [14] and references therein) but has never been reported previously in neighboring odd-odd nuclei.

The complex alignment pattern is very interesting and needs further explanations. One suggestion based on the TRS and CSM calculations attributes the complex alignments to configuration-dependent shape effects. Such calculations have been performed for a number of nuclei in this mass region [12,14,21,44–46]. It has been found that the nuclear shapes evolve within a band in different ways depending on the quasiparticle excitations. The change of deformation along the bands with $\pi 1/2^-[541]$ unoccupied is due to a proton pair scattering from an upsloping orbital ($\pi h_{11/2}$ or $\pi d_{5/2}$) to the $\pi 1/2^-[541]$ downsloping orbital. Thus the $1/2^-[541]$ quasiproton excitation plays an important role for the shape evolution. As pointed out in Ref. [14], the $\pi 1/2^-[541]$ intruder orbital is only partly occupied by the $(h_{9/2})^2_{J=0}$ proton pair at lower rotational frequencies, so that the nucleus will keep its initial shape with smaller $\beta_2$. This intruder orbital is almost fully occupied by the $(h_{9/2})^2_{J=0}$ proton pair at higher frequencies, leading to a larger deformation. Thus the complex alignment as observed in the $\pi 9/2^-[514]$ band of $^{179}$Ir could be interpreted as resulting from a shape change (or the $\beta$-stretching process) from

smaller to larger deformation with increasing rotational frequency. An alternative explanation attributes this feature to three-band interactions. This has been suggested (see Ref. [13] and references therein) to explain the complex alignments in the yrast bands of Os and in the $\pi h_{11/2}$ (and $\pi d_{5/2}$) bands of Re and Ir nuclei. It is worth noting that the neutron $AB$ crossing is blocked in the $\pi 9/2^-[514] \otimes \nu i_{13/2}$ band of $^{180}$Ir. In this case, the neutron pair alignment should correspond to the $BC$ or $AD$ crossings. If the three-band interaction model is applied to band 4, the nature of the $S$ band should be different from that of the $\pi 9/2^-[514]$ band of $^{179}$Ir in which the $AB$ crossing is involved in the associated $S$ band. However, the fact that the dynamic moments of inertia, $J^{(2)}$, have almost the same values in a large frequency range [see Fig. 12(b)] for the $\pi 9/2^-[514]$ and $\pi 9/2^-[514] \otimes \nu i_{13/2}$ bands suggests strongly that the complex alignments in both nuclei have a similar origin.

To summarize, the gradual alignment gain observed in band 4 of $^{180}$Ir can be understood, at least partly, as being due to deformation change with rotation (or the $\beta$ stretching process). This, the $\beta$ stretching process, is caused by proton-pair scattering (coupled to zero spin) into the $1/2^-[541]$ orbital and may not be affected by the extra $i_{13/2}$ neutron in odd-odd $^{180}$Ir. The nuclear shape associated with band 4 in $^{180}$Ir may evolve in the same way as in the $\pi h_{11/2}$ band of $^{179}$Ir. Consequently, similar patterns in the $i_x(\hbar\omega)$ and $J^{(2)}(\hbar\omega)$ plots can exist in both nuclei.

## IV. SUMMARY AND CONCLUSIONS

High-spin states in $^{180}$Ir have been investigated, for the first time, with standard in-beam $\gamma$-ray spectroscopy techniques. A level scheme consisting of five rotational bands has been established. The possible quasiparticle configurations of these bands have been suggested based on the measured in-band $B(M1)/B(E2)$ ratios and the existing knowledge of band structures in the neighboring odd-$A$ and even-$A$ nuclei. The doubly decoupled bands in $^{178-186}$Ir exhibit regular level staggering as a function of neutron-pair number. The first band crossing has been observed in the $\pi 1/2^-[541] \otimes \nu 1/2^-[521]$ and $\pi 1/2^-[541] \otimes \nu 5/2^-[512]$ bands at $\hbar\omega_c = 0.26(1)$ MeV, which is close to the value $> \hbar\omega_c = 0.25(1)$ MeV obtained in the $\nu 1/2^-[521]$ and $\nu 5/2^-[512]$ bands of $^{179}$Os but smaller than $\hbar\omega_c = 0.30$ MeV found in the yrast band of $^{178}$Os. These backbends originate from the neutron $AB$ crossings; the different $\hbar\omega_c(AB)$ values can be interpreted as being due to neutron blocking effects. Neutron $BC$ crossing occurs at $\hbar\omega_c(BC) = 0.31(1)$ MeV in the $\nu i_{13/2}$ band of $^{179}$Os, but shifts to higher frequency above 0.34 MeV in the $\pi 1/2^-[541] \otimes \nu i_{13/2}$ band. This shift in $BC$ crossing frequency may be the consequence of stabilization effects from the $1/2^-[541]$ quasiproton, which is considered to stabilize the nucleus against $\beta$ and $\gamma$ deformations. Two strongly coupled bands show the gradual alignment gains and small shoulders in $J^{(2)}$ at lower rotational frequencies before the first backbending. These features are very similar to those in the $\pi 9/2^-[514]$ and $\pi 5/2^+[402]$ bands of the neighboring odd-$A$ Re and Ir nuclei. All may be caused by shape changes ($\beta$ stretching) associated with $(h_{9/2})^2_{J=0}$ proton-pair excitation.

## ACKNOWLEDGMENTS

The authors wish to thank the staffs in the JAERI tandem accelerator for providing $^{31}$P beam and the staffs of GSI target laboratory (Darmstadt, Germany) for providing the $^{154}$Sm target. This work was supported by the National Natural Sciences Foundation of China (Grant Nos. 10025525 and 19605008), the Japan STA Scientist Exchange Program (Grant No. 1998-21), the JSPS Invitation Fellowship Program for Research in Japan (Grant No. L00515), and the Major State Basic Research Development Program of China (Contract No. G2000077400).

[1] A. J. Kreiner, Nucl. Phys. **A520**, 225c (1990).

[2] R. Bengtsson, H. Frisk, R. F. May, and J. A. Pinston, Nucl. Phys. **A415**, 189 (1984).

[3] R. A. Bark, J. M. Espino, W. Reviol, P. B. Semmes, H. Carlsson, I. G. Bearden, G. B. Hagemann, H. J. Jensen, I. Ragnarsson, L. L. Riedinger, H. Ryde, and P. O. Tjom, Phys. Lett. B **406**, 193 (1997).

[4] M. A. Cardona, A. J. Kreiner, D. Hojman, G. Levinton, M. E. Debray, M. Davidson, J. Davidson, R. Pirchio, H. Somacal, D. R. Napoli, D. Bazzacco, N. Blasi, R. Burch, D. De Acuña, S. M. Lenzi, G. Lo Bianco, J. Rico, and C. Rossi Alvarez, Phys. Rev. C **59**, 1298 (1999).

[5] Y. H. Zhang, T. Hayakawa, M. Oshima, Y. Toh, J. Katakura, Y. Hatsukawa, M. Matsuda, N. Shinohara, T. Ishii, H. Kusakari, M. Sugawara, and T. Komatsubara, Eur. Phys. J. A **8**, 439 (2000).

[6] Fu-Guo Deng, Chun-Xiang Yang, Hui-Bin Sun, Xiao-Guang Wu, Jing-Bin Lu, Guang-Yi Zhao, Guang-Bing Han, Zhao-Hua Peng, Li-Chang Yin, Shu-Xian Wen, Guang-Sheng Li Guan-Jun Yuan, Hong-Yu Zhou, Yun-Zuo Liu, and Li-Hua Zhu, Chin. Phys. Lett. **18**, 888 (2001).

[7] D. Hojman, M. A. Cardona, M. Davidson, M. E. Debray, A. J. Kreiner, F. Le Blanc, A. Burlon, J. Davidson, G. Levinton, H. Somacal, J. M. Kesque, F. Naab, M. Ozafrán, P. Stoliar, M. Vázquez, D. R. Napoli, D. Bazzacco, N. Blasi, S. M. Lenzi, G. Lo Bianco, and C. Rossi Alvarez, Phys. Rev. C **61**, 064322 (2000).

[8] Guangyi Zhao, Yunzuo Liu, Jingbin Lu, Yingjun Ma, Lichang Yin, Xianfeng Li, Zhihuan Li, Xiaoguang Wu, Guangsheng Li, Shuxian Wen, and Chunxiang Yang, Eur. Phys. J. A **9**, 299 (2000).

[9] S. K. Kotoch, S. L. Gupta, S. C. Pancholi, D. Mehta, S. Malik, G. Shanker, L. Chturvedi, and R. K. Bhowmik, Eur. Phys. J. A **4**, 307 (1999).

[10] R. A. Bark, H. Carlsson, S. J. Freeman, G. B. Hagemann, F. Ingebretsen, H. J. Jensen, T. Lönnroth, M. J. Piiparinen, I. Ragnarsson, H. Ryde, H. Schnack-Petersen, P. B. Semmes, and P. O. Tjom, Nucl. Phys. **A630**, 603 (1998).

[11] Y. H. Zhang, S. Q. Zhang, Q. Z. Zhao, S. F. Zhu, H. S. Xu, X. H. Zhou, Y. X. Guo, X. G. Lei, J. Lu, Q. B. Gou, H. J. Jin, Z. Liu, Y. X. Luo, X. F. Sun, Y. T. Zhu, X. G. Wu, S. X. Wen, and C. X. Yang, Phys. Rev. C **60**, 044311 (1999).
[12] J. C. Wells, N. R. Johnson, C. Baktash, I. Y. Lee, F. K. McGowan, M. A. Riley, A. Virtanen, and J. Dudek, Phys. Rev. C **40**, 725 (1989).
[13] G. D. Dracoulis, B. Fabricius, T. Kibèdi, A. M. Baxter, A. P. Byrne, K. P. Libe, and A. E. Stuchbery, Nucl. Phys. **A534**, 173 (1991).
[14] R. Bengtsson, Nucl. Phys. **A520**, 201c (1990).
[15] J. C. Wells, N. R. Johnson, C. Baktash, I. Y. Lee, F. K. McGowan, M. N. Rao, L. L. Riedinger, V. Janzen, W. C. Ma, Shuxian Wen, Ze-Min Chen, P. B. Semmes, G. A. Leander, and Y. S. Chen, Phys. Rev. C **36**, 431 (1987).
[16] L. L. Riedinger, Nucl. Phys. **A520**, 287c (1990).
[17] U. Bosch, W.-D. Schmidt-Ott, F. Meissner, H. Salewski, and R. Michaelsen, Z. Phys. A **341**, 245 (1992).
[18] C. R. Bingham, M. B. Kassim, M. Zhang, A. Akovali, K. S. Toth, W. D. Hamilton, H. K. Carter, J. Kormicki, and M. M. Jarrio, Phys. Rev. C **51**, 125 (1995).
[19] Y. H. Zhang, T. Hayakawa, M. Oshima, J. Katakura, Y. Hatsukawa, M. Matsuda, H. Kusakari, M. Sugawara, and T. Komatsubara, Eur. Phys. J. A **5**, 345 (1999).
[20] K. Furuno, M. Oshima, T. Komatsubara, K. Furutaka, T. Hayakawa, M. Kedera, Y. Hatsukawa, M. Matsuda, S. Mitarai, T. Shizuma, T. Saitoh, N. Hashimoto, H. Kusakari, M. Sugawara, and T. Morikawa, Nucl. Instrum. Methods Phys. Res. A **421**, 211 (1999).
[21] H.-Q. Jin, L. L. Riedinger, C. R. Bingham, M. P. Carpenter, V. P. Janzen, C.-H. Yu, and L. Zhou, P. B. Semmes, J.-Y. Zhang, M. A. Riley, C. Baktash, M. L. Halbert, N. R. Johnson, I. Y. Lee, and F. K. McGowan, Phys. Rev. C **53**, 2106 (1996).
[22] R. Kaczarowski, U. Garg, E. G. Kunk, and J. W. Mihelich, Phys. Rev. C **45**, 103 (1992).
[23] R. B. Lieder, A. Neskakis, J. Skalski, G. Sletten, J. D. Garrett, and J. Dudek, Nucl. Phys. **A476**, 545 (1988).
[24] R. A. Bark, G. B. Hagemann, H. J. Jensen, W. Korten, J. Wrzesinski, H. Carlsson, M. Bergström, A. Brochstedt, A. Nordlund, H. Ryde, P. Bosetti, S. Leoni, F. Ingebretsen, and P. O. Tjom, Nucl. Phys. **A591**, 265 (1995).
[25] Y. H. Zhang, T. Hayakawa, M. Oshima, Y. Toh, J. Katakura, Y. Hatsukawa, M. Matsuda, N. Shinohara, T. Ishii, H. Kusakari, M. Sugawara, and T. Komatsubara, Chin. Phys. Lett. **18**, 27 (2001).
[26] A. J. Kreiner, J. Davidson, M. Davidson, P. Thieberger, and E. K. Warburton, Phys. Rev. C **42**, 878 (1990).
[27] A. J. Kreiner, P. Thieberger, and E. K. Warburton, Phys. Rev. C **34**, 1150 (1986).
[28] A. J. Kreiner, D. E. Di Gregorio, A. J. Fendrik, J. Davidson, and M. Davidson, Phys. Rev. C **29**, 1572 (1984).
[29] S. Drissi, A. Bruder, M. Carlen, J. Cl. Dousse, M. Gasser, J. Kern, S. J. Mannanal, B. Perny, Ch. Rheme, J. L. Salicio, J. P. Vorlet, and I. Hamamoto, Nucl. Phys. **A543**, 495 (1992).
[30] R. W. Hoff, J. Kern, R. Piepenbring, and J. P. Boisson, in *Capture Gamma-Ray Spectroscopy and Related Topics—1984*, edited by S. Raman, AIP Conf. Proc. No. 125 (AIP, New York, 1985), p. 274.
[31] A. K. Jain, R. K. Sheline, D. M. Headly, P. C. Sood, D. G. Burke, I. Hrivnácová, J. Kvasil, D. Nosek, and R. W. Hoff, Rev. Mod. Phys. **77**, 843 (1998).
[32] D. L. Balabanski, R. M. Lieder, T. Kutsarova, W. Gast, G. Hebbinghaus, A. Krámer-Flecken, T. Rzaca-Urban, H. Schnare, W. Urban, G. Sletten, K. H. Maier, and K. O. Zell, Nucl. Phys. **A563**, 129 (1993).
[33] J. Burde, M. A. Deleplanque, R. M. Diamond, A. O. Macchiavelli, F. S. Stephens, and C. W. Beausang, Phys. Rev. C **46**, 1642 (1992).
[34] G. D. Dracoulis, C. Fahlander, and A. P. Byrne, Nucl. Phys. **A401**, 490 (1983).
[35] M. J. A. De Voigt, R. Kaczarowski, J. H. Riezebos, R. F. Noorman, J. C. Bacelar, M. A. Deleplanque, R. M. Diamond, and F. S. Stephens, Nucl. Phys. **A507**, 447 (1990).
[36] A. Bohr and B. R. Mottelson, *Nuclear Structure* (Benjamin, New York, 1975), p. 44.
[37] J. Kern and G. L. Struble, Nucl. Phys. **A286**, 371 (1977).
[38] S. Raman, C. W. Nestor, S. Kahane, and K. H. Bhatt, At. Data Nucl. Data Tables **42**, 1 (1989).
[39] J. Burde, A. O. Macchiavelli, M. A. Deleplanque, R. M. Diamond, F. S. Stephens, C. W. Beausang, R. J. McDonald, and J. E. Draper, Phys. Rev. C **38**, 2470 (1988).
[40] J. D. Garret and S. Frauendorf, Phys. Lett. **108B**, 77 (1982).
[41] R. Bengtsson, S. Frauendorf, and F.-R. May, At. Data Nucl. Data Tables **35**, 15 (1986).
[42] W. Nazarewich, M. A. Riley, and J. D. Garrett, Nucl. Phys. **A512**, 61 (1990).
[43] S.-X. Wen, H. Zheng, S.-G. Li, G.-S. Li, G.-J. Yuan, P.-F. Hua, P.-K. Weng, L.-K. Zhang, P.-S. Yu, C.-X. Yang, H.-B. Sun, Y.-B. Liu, Y.-Z. Liu, Y. Sun, and D.H. Feng, Phys. Rev. C **54**, 1015 (1996).
[44] J. Nyberg, A. Johnson, M. P. Carpenter, C. R. Bingham, L. H. Courtney, V. P. Jansen, S. Juutinen, A. J. Larabee, Z.-M. Liu, L. L. Riedinger, C. Baktash, M. L. Halbert, N. R. Johnson, I. Y. Lee, Y. Schutz, J. C. Waddington, and D. G. Popescu, Nucl. Phys. **A511**, 92 (1990).
[45] M. P. Carpenter, C. R. Bingham, L. H. Courtney, V. P. Janzen, A. J. Larabee, Z.-M. Liu, L. L. Riedinger, W. Schmitz, R. Bengtsson, T. Bengtsson, W. Nazarewicz, J.-Y. Zhang, J. K. Johansson, D. G. Popescu, J. C. Waddington, C. Baktash, M. L. Halbert, N. R. Johnson, I. Y. Lee, Y. S. Schutz, J. Nyberg, A. Johnson, R. Wyss, J. Debuc, G. Kajrys, S. Monaro, S. Pilotte, K. Honkanen, D. G. Sarantites, and D. R. Haenni, Nucl. Phys. **A513**, 125 (1990).
[46] R. Wyss, W. Satula, W. Nazarewicz, and A. Johnson, Nucl. Phys. **A511**, 324 (1990).
[47] Y. H. Zhang, S. Q. Zhang, W. X. Huang, X. H. Zhou, X. C. Feng, X. Xu, X. G. Lei, Y. X. Guo, S. F. Zhu, J. J. He, Z. Liu, S. J. Wang, and Y. X. Luo, Eur. Phys. J. A **7**, 19 (2000).
[48] A. J. Kreiner, V. R. Vanin, F. A. Beck, Ch. Bourgeois, Th. Byrski, D. Curien, G. Duchêne, B. Haas, J. C. Merdinger, M. G. Porquet, P. Romain, S. Rouabah, D. Santos, and J. P. Vivien, Phys. Rev. C **40**, R487 (1989).
[49] Yunzuo Liu, Jingbin Lu, Yingjun Ma, Shangui Zhou, and Hua Zheng, Phys. Rev. C **54**, 719 (1996).
[50] Yunzuo Liu, Yingjun Ma, Hongting Yang, and Shangui Zhou, Phys. Rev. C **52**, 2514 (1995).